OSBP-mediated PI(4)P-cholesterol exchange at endoplasmic reticulum-secretory granule contact sites controls insulin secretion

Styliani Panagiotou[1], Phuoc My Nguyen[1#], Kia Wee Tan[1#], Andreas Müller[2,3,4], Anna Wendt[5,6], Lena Eliasson[5,6], Anders Tengholm[1], Michele Solimena[2,3,4] and Olof Idevall-Hagren[1*]

[1] Department of Medical Cell Biology, Uppsala University, Uppsala, Sweden; [2] Molecular Diabetology, University Hospital and Faculty of Medicine Carl Gustav Carus, TU Dresden, Dresden, Germany; [3] Paul Langerhans Institute Dresden (PLID) of the Helmholtz Center Munich at the University Hospital Carl Gustav Carus and Faculty of Medicine of the TU Dresden, Dresden, Germany; [4] German Center for Diabetes Research (DZD e.V.), Neuherberg, Germany; [5] Department of Clinical Sciences, Lund University, Lund, Sweden; [6] Lund University Diabetes Center (LUDC).

[#]Equal contribution. [*]Correspondence: olof.idevall@mcb.uu.se

Insulin secretion is the process whereby insulin-containing granules fuse with the plasma membrane of β-cells. Exocytosis is preceded by cargo loading, maturation and transport of the secretory granules; processes that require modification of both the protein and lipid composition of the granules. We recently identified phosphatidylinositol-4 phosphate (PI[4]P) dephosphorylation by INPP5F/Sac2 on the surface of insulin granules as a key step that precedes stable granule docking at the plasma membrane and that is required for normal insulin secretion. Here, we show that PI(4)P is used to target the lipid exchange protein oxysterol-binding protein (OSBP) to the granule surface where it is involved in PI(4)P/cholesterol exchange. Loss of Sac2 resulted in excess accumulation of cholesterol on insulin granules that was normalized when OSBP expression was reduced. Acute inhibition of OSBP resulted in dramatic cellular redistribution of OSBP to insulin granules where it colocalized with the ER-resident protein VAP-A at ER-granule contact sites. Stimulation of insulin secretion also resulted in translocation of OSBP to the insulin granule surface in a process that depended on Ca^{2+}-induced acidification of the cytosol. Similar to Sac2 knockdown, inhibition of OSBP suppressed insulin secretion without affecting insulin production. In conclusion, we show that lipid exchange at ER-granule contacts sites is involved in the exocytic process, and propose that these contacts act as reaction centers with multimodal functions during insulin granule maturation.

INTRODUCTION

Blood glucose homeostasis critically depends on the appropriate release of insulin from pancreatic β-cells. Insulin is produced as a pro-peptide that is packaged into secretory granules that bud from the trans-Golgi network. These immature granules undergo a series of maturation steps that involve changes in the composition of both granular lipids and proteins and that coincide with the maturation of insulin (Omar-Hmeadi and Idevall-Hagren, 2021). A typical β-cell contains between 5000-15000 secretory granules (SGs) (Müller et al., 2021; Sato Tamiko, 1981), but only around 50-100 of these have the ability to fuse with the plasma membrane (Barg et al., 2002; Olofsson et al., 2002). These granules belong to the readily-releasable pool and are situated at the plasma membrane where they await a triggering Ca^{2+}-

signal. Prolonged stimulation of insulin secretion will deplete this pool and new SGs have to be recruited from the large reserve pool to sustain secretion. This recruitment primarily involves newly synthesized SGs and depends on granule transport along microtubules as well as acquisition of specific priming and docking factors and interactions with components of the secretory machinery, including t-SNARE family members and voltage-dependent Ca^{2+} channels (Barg et al., 2002; Barg et al., 2010; Bokvist et al., 1995; Bracey et al., 2020; Hoboth et al., 2015; Ivanova et al., 2013). Defects in the replenishment of release-competent SGs have been observed in type-2 diabetes and likely contribute to disease development (Gandasi et al., 2018).

The mechanisms by which SGs dock and fuse with the plasma membrane are well-characterized and to a large extent similar to those of other neuro-endocrine cells. However, the steps preceding the granules' arrival at the plasma membrane are largely unclear. These steps include the action of numerous small GTPases, including Rab3, Rab27 and Rab2, and the corresponding Rab-effectors, but it is not well understood how these reactions are regulated (Omar-Hmeadi and Idevall-Hagren, 2021). Progression through the endo-lysosomal system requires the cooperative action of Rabs and phosphoinositides, which together controls the recruitment of both phosphoinositide-metabolizing enzymes and Rab effectors and ensures unidirectionality throughout the membrane trafficking cascade (Di Paolo and De Camilli, 2006). To what extent the same principle guide progression through the regulated secretory pathway is not known. The trans-Golgi network is rich in phosphatidylinositol 4-phosphate (PI(4)P), and this lipid is directly involved in the formation of nascent SGs via recruitment of the GTPase Arf1 (Cruz-Garcia et al., 2013; Dittié et al., 1996). The membrane of the newly formed SGs likely contains high concentrations of PI(4)P, both as a consequence of its Golgi origin and through the action of PI4-kinases (Olsen et al., 2003). We recently described the involvement of the PI(4)P phosphatase Sac2 in insulin SG maturation and exocytosis (Nguyen et al., 2019). Lack of Sac2 resulted in accumulation of PI(4)P on the SG surface and in an inability of granules to stably dock and fuse with the plasma membrane. This mechanism resembles vesicle maturation in yeast cells, where the ER-localized PI(4)P phosphatase Sac1 is recruited to the vesicle surface (Ling et al., 2014). In these cells, recruitment occurs through an interaction with the lipid transport protein Osh4p, which also directly contributes to PI(4)P removal by exchanging it for cholesterol (de Saint-Jean et al., 2011; Ling et al., 2014). To what extent a similar mechanism operates during regulated secretion of insulin is not known. However, observations that loss of the mammalian Osh4p homologue OSBP leads to impaired insulin secretion and that SG cholesterol accumulation is required for insulin release are consistent with the existence of such a mechanism (Hao et al., 2007; Hussain et al., 2018; Xia et al., 2008).

We now show that loss of Sac2 in β-cells results in excess accumulation of cholesterol on the surface of insulin SGs through an OSBP-dependent process. Recruitment of OSBP to the granule surface is controlled by granular PI(4)P and dynamically regulated by cytosolic Ca^{2+} and pH, and knockdown or inhibition of OSBP results in impaired insulin secretion. These results unravel a SG maturation pathway in β-cells that resembles that previously described for constitutive secretion in yeast cells, and also demonstrate for the first time a role of ER-SG contact sites in regulated secretion.

MATERIALS AND METHODS

Reagents and plasmids

TopFluor Cholesterol (23-[dipyrrometheneboron difluoride]-24-norcholesterol was from Avanti Polar Lipids, Inc. Cholesterol Assay Kit (Cell-Based) was from Abcam (Ab122116).

OSW-1 was from Cayman Chemical. Cal-590-AM and Cal520-AM were from AAT Bioquest. BCECF was from Life technologies. Plasmids pLJM1-FLAG-GFP-OSBP was from Addgene (Plasmid #134659; (Lim et al., 2019)), GFP-Sac2 and VAPA-GFP were gifts from Pietro De Camilli (Yale University, New Haven, CT; (Nakatsu et al., 2015)) GFP-Rab3a, NPY-mCherry, NPY-mNG and VAMP2-pHluorin were gifts from Sebastian Barg, Uppsala University, Sweden. RA-Sec61β and GB-Dcp1 were gifts from Gia Voeltz (Addgene plasmid #153978, #153979). Halo-OSBP was created by amplifying OSBP from pLJM1-FLAG-GFP-OSBP (Addgene #134659) and inserting it by Gibson Assembly (New England Biolabs) into the BglII/NotI sites of a customized cloning vector bearing an N-terminal Halo-tag (pENTR20-Halo-C1). This vector was recombined using Gateway LR reaction (Invitrogen) into a customized Gateway-enabled pCDH vector (System Biosciences) and expressed under control of a EF1α promoter. GB-Rab3 was created by amplifying mouse Rab3a ORF and inserting it into the XhoI/SacII site of the GB-Dcp1 using the following primers: FW: 5'-GATCTCGAGTACCGGTTGGATCAGGATCAATGGCCTCAGCCACAGAC-3' RV: 5'-GGGCCCGCGGTCAGCAGGCGCAATCC-3'. GB-OSBP was generated by amplifying OSBP from Halo-OSBP using the following primers: FW: 5'-CAAGTCCGGACTCAGATCCATGGCTGCTACGGAGC-3', RV: 5'-CAGTTATCTAGATCCGGTGGATCTCAGAAAATGTCCGGGCATG-3' followed by ligation to pGB-Dcp1 using Xho1/Xma1. GB-CAAX was generated by releasing Rab3 from GB-Rab3 with Nhe1/Age1 followed by ligation to pCIBN-CAAX (Idevall-Hagren et al., 2012). RA-CAAX was generated by releasing RA from RA-Sec61β with Nhe1/Age1 followed by ligation to pGB-CAAX. GB-E-Syt3 was generated by releasing E-Syt3 from pEGFP-E-Syt3 (Giordano et al., 2013) with Nhe1/Xho1 followed by ligation to pGB-Dcp1. E-Syt3-GB was generated by releasing E-Syt3 from pE-Syt3-EGFP (Giordano et al., 2013) with Nhe1/Age1 followed by ligation to pTOM20-GB (Xie et al., 2022). RA-Rab3 was generated by releasing Rab3 from GB-Rab3 with Xho1/SacII followed by ligation to pRA-Sec61β (Lee et al., 2020). GB-Sec61β was generated by releasing GB from pGB-Dcp1 (Lee et al., 2020) with Nhe1/Xho1 followed by ligation to pRA-Sec61β. Adenoviral particles (E5 serotype) carrying RA-Sec61β and GB-Rab3a under the control of CMV-promoters were produced by Vector Biolabs (Malvern, PA). The following antibodies were used in the study: OSBP Polyclonal (catalogue no. PA5-30110, host: rabbit, 1:300, Invitrogen), VAPA polyclonal (HPA009174, Atlas Antibodies, host: Rabbit, 1:400), VAPB polyclonal (HPA013144, Atlas Antibodies, host: Rabbit, 1:400), PI4K2A monoclonal (sc-390026, Santa Cruz, host: mouse, 1:100), β-actin monoclonal (clone C4, sc-47778, Santa Cruz Biotechnology, host: mouse, 1:300), IP3R1 polyclonal (catalogue no. ab264281, Abcam, host: rabbit, 1:500), Rab3 monoclonal (catalogue no. 107 111, Synaptic Systems, host: mouse, 1:500), Chromogranin A polyclonal (catalogue no. 10529-1-AP, Proteintech, host: Rabbit, 1:400), insulin polyclonal (catalogue no. A0564, Dako, host: guinea pig, 1:1000), calnexin (PA5-34754, Invitrogen, host: Rabbit, 1:500), GolgB1 (BS-13356R, Bioss, host: rabbit, 1:500).

Cells and transfection

MIN6 cells were used between passages 18 to 35 and kept in cell culture medium composed of DMEM supplemented with 4.5g/L glucose, 2mM L-glutamine, 100U/mL Penicillin, 100μg/mL Streptomycin, 50μM 2-mercaptoethanol, and 15% fetal bovine serum (all from Life Technologies). The cells were cultured in a humidified atmosphere at 37°C and 5% CO_2. Reverse transfections were carried out in 100μL of OptiMEM with 0.5μL Lipofectamine 2000 or Lipofectamin 3000 (all from Life Technologies), 0.1-0.4μg plasmid DNA, and 200,000 cells. The transfection was terminated after 3-5 h, and imaging was done between 22 and 30 hours after transfection.

Viral transduction of MIN6 cells.
MIN6 cells were infected with 10 µl of high titration virus in 100 µL of culture medium (RA-Sec61b;5.5x10^{10} PFU/mL, GB-Rab3;4.5x10^{10} PFU/mL; Vector Biolabs, Malvern, PA). After 3 h, the coverslips were washed with medium and the cells were cultured for at least two days to allow the expression of the contact sites reporter before performing experiments.

Pancreatic islet isolation and culture
All animal experimental procedures were approved by the local ethics committee for use of laboratory animals in Uppsala, Sweden. Islets of Langerhans were isolated from 4–12-month-old C57Bl6J mice by collagenase digestion of the pancreas followed by hand-picking of individual islets. After isolation, the islets were cultured for 1-3 days in RPMI 1640 medium containing 5.5 mM glucose, 10% fetal calf serum, 100 U/mL penicillin and 100 µg/mL streptomycin at 37°C in a 5% CO_2 humidified atmosphere. 20-50 freshly isolated islets were infected with 10 µl of high titration virus in 100 µL of culture medium (RA-Sec61b;5.5x10^{10} PFU/mL, GB-Rab3;4.5x10^{10} PFU/mL; Vector Biolabs, Malvern, PA). After 3 h, the coverslips were washed with medium and the cells were cultured for at least two days to allow the expression of the contact sites reporter before performing experiments. Human islets were isolated from the pancreas of cadaveric organ donors by the Nordic Network for Clinical Islet Transplantation Uppsala (ethical approval by Uppsala Regional Ethics Board) with written donor and family consent for use in research. Work with human tissue complied with all relevant ethical regulations for use of human tissue in research and the study was approved by the Uppsala Regional Ethics Board (2006/348). Isolated islets were cultured free-floating in sterile dishes in CMRL 1066 culture medium containing 5.5 mM glucose, 10% fetal calf serum (FCS), 2 mM l-glutamine, streptomycin (100 U/ml), and penicillin (100 U/ml) at 37 °C in an atmosphere of 5% CO_2 for up to 2 weeks.

siRNA-mediated knockdown
Sac2 knockdown was performed with siRNA targeting mouse gene sequence Inpp5f: 5'-GGAAUGCGGUAUAAACGAATT-3' and was from Ambion (Life Technologies). OSBP knockdown was performed using ON-TARGET plus SMART pool Mouse OSBP siRNA from Dharmacon (). MIN6 cells were transfected in 12 well-plates with siRNA using Lipofectamine 2000, followed by a second round of transfection 3-4 hours later using RNAiMax (Life Technologies) according to the manufacturer's instructions with final siRNA concentration of 50 nM and 20 nM for Sac2 and OSBP, respectively. ON-TARGET plus NON-targeting Pool from Dharmacon was used as control.

Quantatitive RT-PCR
Sac2 knockdown was confirmed by quantitative RT-PCR using QuantiTect SYBR Green RT-PCR kit (Qiagen) and the following primers: Sac2-fwd: 5'TAAGGAGAGCCAGAGAAGCCA-3', Sac2-rev: 5-CAGCAGCACTTCCACATCTCT-3'; GAPDH-fwd: 5'-ACTCCACTCACGGCAAATTC-3'; GAPDH-rev: 5'-TCTCCATGGTGGTGAAGACA-3'. PCR reactions were performed using Light Cycler 2.0 (Roche). Results are expressed as ΔΔCt, normalized to the expression in control samples.

Western blot
Cells were lysed on ice with RIPA buffer (50 mM Tris-HCl, pH 7.4, 1% NP-40, 0.5% Na-deoxycholate, 0.1% SDS, and 10% EDTA) supplemented with a protease inhibitor cocktail (Roche). Samples were cleared by centrifugation and protein concentration was measure by the Bradford assay. OSBP knockdown was confirmed by Western blotting using OSBP

Polyclonal Antibody (1:1000, Invitrogen) and β-actin mouse monoclonal (clone C4, sc-47778, 1:300, Santa Cruz Biotechnology).

Immunofluorescence

Cells grown on monolayers were fixed in 4% paraformaldehyde in either PBS or PHEM buffer (60mM PIPES, 25mM HEPES, 10mM EGTA, 4mM MgSO4, pH 6.9) for 20 mins at RT, followed by 3 washes of buffer. Permeabilization was performed using 0.1-0.2% Triton X-100 for 10-15mins, followed by 3 washes of buffer, and followed by blocking for 1hr in buffer containing 2% BSA. Primary antibody incubation was carried out overnight at 4°C in blocking buffer, washed 3 times and incubated for 1hr with secondary antibody in blocking buffer. Coverslips were then washed 3 times, mounted in Prolong Glass (Invitrogen) and left to dry for at least 18hr before imaging. Where NPY-mNeonGreen was visualized in fixed samples, the secondary antibody incubation included 5nM of Fluotag-X2-anti-mNeonGreen conjugated to Atto488 (Nanotag Biotechnologies).

Cholesterol visualization

TopFluor cholesterol was diluted (0.6 mg/mL) in methanol:water (95:5 vol%) followed by sonication. The dissolved cholesterol was transferred to glass tubes and dried under N_2, followed by resuspension in 4 mg/mL fatty acid free BSA. MIN6 cells were loaded with 1μM TopFluor cholesterol and incubated for 3 hours followed by additional culture in a cholesterol-free medium for 15-18 hours prior live cell imaging. Filipin cholesterol staining was performed following the manufacturer's instructions (Ab122116 - Cholesterol Assay Kit, Abcam) and imaging was performed 0-4 hours after staining.

Measurements of intracellular Ca^{2+} and pH

To measure changes in the intracellular Ca^{2+} concentrations, MIN6 cells or mouse islets were preincubated at 37°C for 30 min in an experimental buffer (see below) supplemented with 2 μM of the AM-ester-form of the Ca^{2+}-indicator Cal-520. The cells were subsequently washed twice with experimental buffer before visualization by fluorescence microscopy (excitation 491 nm, emission 530/50 nm). Intracellular pH was determined using the ratiometric dye BCECF. MIN6 cells were incubated with 2 μM of the AM-ester-form of BCECF for 30 min at 37°C, followed by two washing steps to remove residual indicator and visualization by fluorescence microscopy (excitation 442 nm and 491 nm, emission 530/50 nm).

Insulin secretion measurements

MIN6 cells were cultured in 12-well plates to approximately 70% confluency. Cells were washed three times with PBS, pre-incubated in experimental buffer (125mM NaCl, 4.9mM KCl, 1.2mM $MgCl_2$, 1.3mM $CaCl_2$, 25mM Hepes, and 0.1% BSA) with 3mM Glucose for 30 min at 37°C. Cells were then incubated for 30 min in experimental buffer with 3mM glucose, 20mM glucose or 3mM glucose and 30 mM KCl. The supernatants were collected for insulin measurement using a Mouse Insulin ELISA kit (Mercodia, Uppsala, Sweden). Isolated mouse islets of Langerhans (8-10 islets per experiment) were placed in a closed 10 μL chamber made of Teflon tubing with a fine mesh plastic net at the outlet that prevented the islets from escaping. Islets were subsequently perfused with experimental buffer. The perfusate was collected in 5 min fractions and insulin content in the fractions was determined using a mouse insulin ELISA kit (Mercodia). Cells were subsequently collected, diluted in acidic ethanol (75% EtOH and 15% HCl) and sonicated for 2x10 s to determine the insulin content.

OSW-1 treatment

Cells were incubated in experimental buffer containing either 0.1% DMSO or 20nM OSW-1 (dissolved in DMSO) for 30 min at 37°C before imaging or ELISA sample collection.

Proximity ligation assay

PLA was performed according to the manufacturer's recommendation (Navinci™ NaveniFlex MR). Primary antibodies against IP3R1 (ab264281, rabbit polyclonal, Abcam) and Rab3 (catalog no. 107 111, mouse monoclonal, Synaptic Systems) were used at 1:500 dilution.

Fluorescence microscopy

All experiments, unless otherwise stated, were performed at 37°C in an experimental buffer containing 125 mM NaCl, 4.9 mM KCl, 1.2 mM $MgCl_2$, 1.3 mM $CaCl_2$, 25 mM Hepes, 3 mM D-Glucose, and 0.1% BSA (pH 7.40). Cells were preincubated in imaging buffer for 30 min before experiments, and continuously perfused with the same buffer at the stage of the microscope. Where required, Halo-tagged proteins were labeled with 40nM of Halo-tag ligand bearing JFX646 (Grimm et al., 2021) for 20 min in experimental buffer and unbound ligand was washed out for 10 min in the same buffer. Confocal microscopy was performed on a Nikon Eclipse Ti-2 equipped with a Yokogawa CSU-10 spinning disc confocal unit and a 100×/1.49-NA plan Apochromat objective (Nikon) as previously described (Idevall-Hagren et al., 2013). Briefly, excitation light was provided by 491-nm, 561-nm DPSS lasers and 640-nm diode laser (all from Cobolt), and fluorescence was detected through interference filters 530/50-nm (GFP, mNG, Alexa488), 590/20-nm (mCherry, RA, Alexa561) or 650LP filter (JF646) with a back-illuminated EMCCD camera (DU-888; Andor Technology) controlled by MetaFluor software (Molecular Devices). TIRF microscopy was performed on two different setups. A custom-built prism-type TIRF microscope equipped a 16×/0.8-NA water-immersion objective (Nikon) was used for low-magnification imaging of cell populations as previously described (Idevall-Hagren et al., 2013). It is built around an E600FN upright microscope (Nikon) contained in an acrylic glass box thermostated at 37°C by an air stream incubator. DPSS lasers (Cobolt) provided 491- nm and 561-nm light for excitation of GFP and mCherry. The laser beams were merged with dichroic mirrors (Chroma Technology), homogenized, and expanded by a rotating Light Shaping Diffuser (Physical Optics) before being refocused through a modified quartz dove prism (Axicon) with a 70° angle to achieve total internal reflection. Laser lines were selected with interference filters (Semrock) in a motorized filter wheel equipped with a shutter (Sutter Instruments) blocking the beam between image captures. Fluorescence from the cells was detected at 530/50 nm for GFP (Semrock interference filters) or 597LP for mCherry (Melles Griot glass filter) with a EM-CCD camera (Andor DU-887) under MetaFluor software control. TIRF imaging was also performed on an inverted Nikon Ti-E equipped with a TIRF illuminator and a 60X 1.45-NA objective (all Nikon). Excitation light was provided by diode-pumped solid-state lasers (491-nm, 561-nm) or diode lasers (640-nm; all from Cobolt). Lasers were merged with dichroic mirrors (Chroma technologies) and excitation light was selected with bandpass filters mounted in a filter wheel (Sutter Instruments Lambda 10-3) and delivered to a fiber optic cable and delivered to the TIRF illuminator. Excitation light was reflected through the objective with a dichroic mirror (ZET405/488/561/640m-TRFv2, Chroma Technologies) and emission light was separated using interference (530/50 nm, 590/20-nm) or longpass (650LP) filters (Semrock) mounted in a filter wheel (Sutter instruments Lambda 10-3). An electronic shutter was used to block light exposure between image captures. Emission light was detected using an Orca-AR camera controlled by MetaFluor software (Molecular Devices Corp.). Filipin imaging was visualized on a laser scanning confocal microscope (Zeiss LSM 780) equipped with a Plan-Apo 20X/0.8-NA objective using a 405-nm diode laser.

Electron microscopy

Mouse or human islets were hand-picked under a microscope and groups of ~50 isolated islets were fixed in Millonig's buffer with 2.5% glutaraldehyde overnight, post-fixed in 1.0% osmium tetroxide, dehydrated and embedded in AGAR 100 (Oxfors Instruments Nordiska AB, Sweden). Before visualization 70–90 nm sections were cut, mounted, and contrasted. The samples were examined in a JEM 1230 electron microscope (JEOL-USA, Inc, MA, USA).

3D segmentation of ER-insulin SG contact sites

Segmentation of ER-SG contact sites was performed on focused ion beam electron microscopy (FIB-SEM) volumes of isolated mouse pancreatic islets previously acquired for and available via the openorganelle platform (https://openorganelle.janelia.org/) under a CC BY 4.0 license (Xu et al., 2021). Small volumes with contact sites were cut in FIJI (Schindelin et al., 2012) and manual segmentation of ER and SG was performed with the Labkit FIJI plugin (Arzt et al., 2022). Ribosomes were segmented by black-and-white-thresholding in Microscopy Image Browser (Belevich et al., 2016). Segmentation results were rendered with ORS Dragonfly (https://www.theobjects.com/dragonfly/index.html).

Image analysis

TIRF microscopy images were analyzed offline using ImageJ. Briefly, for analysis of VAMP2-pHluorin and Cal-520 experiments, cell footprints were manually identified and regions of interest covering the edges of the adherent cells were drawn. Intensity changes within these regions during the experiments were measured and exported to Excel. All data points were background corrected, followed by normalization to the pre-stimulatory level (F/F0). Analysis of enrichment of tagged proteins to insulin SGs was performed using a pipeline assembled in Cell Profiler. Insulin SGs were segmented using the NPY channel. Cells positive for the protein of interest were segmented and all insulin SGs not in an OSBP-positive cell were discarded. The median fluorescence in a 2-pixel wide ring around each insulin SG was defined as the background and the enrichment of the protein of interest was calculated by dividing the mean of fluorescence in each insulin granule with its corresponding background. To determine the percentage of insulin SG positive for a protein, we set the enrichment threshold at 2 standard deviations from the mean. For each treatment, the standard deviations for the basal condition were computed and used for their corresponding treatment conditions.

Statistical analysis

Statistical analysis was performed using 2-way ANOVA followed by Tukey's or Kruskall-Wallis (for non-parametric data) posthoc tests. Where a single test group was compared against a treatment group, we performed Student's 2-tailed unpaired t-test or Mann-Whitney U-test (for non-parametric data). Paired analysis was performed with Student's 2-tailed paired t-test. We did not perform a power analysis and the experiments did not have a predetermined sample size, but this was instead chosen based on experience. At least three independent experiments (performed on separate days) were used for all analyses.

RESULTS

Sac2 regulates cellular cholesterol distribution

The phosphatidylinositol 4-phosphatase (PI[4]P) Sac2 localizes to vesicular structures, including endosomes and SGs (Cao et al., 2020; Hsu et al., 2015; Nakatsu et al., 2015;

Nguyen et al., 2019). Expression of fluorescently tagged Sac2 (mCherry-Sac2) in clonal insulin-secreting MIN6 β-cells followed by confocal microscopy visualization showed the expected colocalization between the lipid phosphatase and a marker of insulin SGs (GFP-Rab3a; Fig. 1A). SGs are also a major storage site for cellular cholesterol (Galli et al., 2023), shown here by the strong colocalization between the fluorescent cholesterol marker filipin and the SG marker NPY-GFP (Fig. 1B). PI(4)P has been shown to be involved in cholesterol transport between organelle membranes (reviewed in (Antonny et al., 2018)). We therefore examined the relationship between Sac2 and cholesterol distribution. Control cells and cells with reduced Sac2 expression (Sac2-KD; Fig. 1C) were transfected with the SG marker NPY-mCherry and visualized by confocal microscopy following incubation with fluorescently labelled cholesterol (Bodipy-chol). We found that cholesterol accumulated on SGs, and that this accumulation was more pronounced in Sac2-KD cells (0.117 for control, 0.161 for Sac2-KD, n=25-26 cells, $P < 0.05$; Fig. 1D-G). Similar results were obtained when cholesterol distribution was instead determined in fixed cells using the fluorescent cholesterol dye Filipin (control = 98 ± 3, Sac2-KD = 136 ± 5, n = 54, $P < 0.001$; Fig. 1H-J). Together, these findings indicate an involvement of Sac2 in the delivery of cholesterol to SGs.

OSBP localizes to insulin SGs in a PI(4)P-dependent manner

PI(4)P-dependent cholesterol transport has been described in both yeast cells and mammalian cells and is mediated by Osh and OSBP/ORP proteins, respectively (Antonny et al., 2018). They function as co-transporters, exchanging PI(4)P for cholesterol in target membranes. OSBP is a major PI(4)P metabolizing enzyme that associates with the ER through an interaction between its FFAT-motif and VAP proteins in the ER membrane and with target membranes through an interaction between its PH-domain and PI(4)P (Levine and Munro, 2002; Mesmin et al., 2013; Wyles et al., 2002). It primarily localizes to the ER-Golgi interface where it exchanges Golgi PI(4)P for ER cholesterol, resulting in removal of PI(4)P through subsequent dephosphorylation by the ER-resident PI(4)P-phosphatase Sac1 (Mesmin et al., 2013; Mesmin et al., 2017). Confocal microscopy imaging of MIN6 β-cells expressing fluorescently tagged OSBP (OSBP-GFP or OSBP-Halo^{JF646}) and an SG marker NPY (NPY-mCherry or NPY-mNG) showed little colocalization, although 2-5% of the granules were found in close apposition to OSBP-positive structures (Fig. 2A-C and Suppl. Fig. 1). Strikingly, addition of the OSBP inhibitor OSW-1 (20 nM) resulted in rapid enrichment of OSBP on SGs, with around 20-30% of the granules being positive for OSBP after 30 min incubation with OSW-1 ($P<0.0001$ for comparison to control; Fig. 2B-E and Suppl. Fig. 1). Granular accumulation in response to OSW-1 was also seen for the PH-domain of OSBP, showing that the interaction with SGs involves binding to PI(4)P (Suppl. Fig. 1). The initial recruitment (minutes) involved a cytosolic pool of OSBP, while prolonged incubation with OSW-1 resulted in a gradual loss of OSBP from the Golgi that was accompanied by further enrichment at the SGs. These results indicate involvement of OSBP in PI(4)P-cholesterol exchange at the surface of SGs and suggest the existence of previously uncharacterized membrane contact sites between the ER and SG. To test this assumption, we expressed the ER-localized OSBP receptor VAP-A fused to GFP or Halo^{JF646} together with NPY-mCherry or NPY-mNG and visualized their distribution under control conditions and after application of OSW-1. VAP-A was homogenously distributed throughout the ER, including ER domains that were in proximity to SGs, and the addition of OSW-1 had little effect on the overall VAP-A distribution, although in some cells we observed strong enrichment of VAP-A around SGs (Fig. 2D, E and Suppl. Fig. 1). We previously showed that the localization of Sac2 to SGs primarily involves the action of a granule-localized PI4-kinase (Nguyen et al., 2019), and consistent with that we now find that the OSW-1-induced recruitment of OSBP to insulin SGs is inhibited by the broad PI4-kinase inhibitor phenylarseneoxide (PAO) but not by the more

selective class IIIβ (PIK93 and PI4KI) or class IIIα (GSK-A1) inhibitors (Fig. 2F-G and Suppl. Fig. 1). Immunostainings as well as live cell imaging revealed the presences of class IIα PI4-kinases on insulin SGs, making this a likely candidate for maintaining the granular PI(4)P pool (Fig. 2H). To determine the distribution of endogenous OSBP and VAP-A/B in relation to insulin granules we immunostained both MIN6 cells and mouse pancreatic islets of Langerhans, treated or not with 20 nM OSW-1 for 30 min, against insulin and OSBP/VAP-A/VAP-B. Under control conditions, OSBP localized to a perinuclear compartment and showed little overlap with SGs while VAP-A and VAP-B showed a reticular distribution and was frequently found close to or at SGs (Fig. 2I-L). OSW-1 treatment resulted in redistribution of OSBP, which now exhibited a punctate distribution and partially overlapped with SGs (Fig. 2I-L). VAP-A and VAP-B were less affected by OSW-1 treatment, although clear punctate localization that overlapped with SGs became more frequent, especially for VAP-B (Fig. 2I). Importantly, OSW-1 treatment was without effect on the overall Golgi and ER morphologies, as determined by immunostainings with GolgB1 (Golgi) and Calnexin (ER) antibodies (Suppl. Fig. 2).

ER-SG contact sites

The localization of both OSBP and VAP-A to SGs indicate the existence of physical contacts between the ER and granules, similar to those previously described at the ER-Golgi, ER-lysosome and ER-endosome interfaces (Dong et al., 2016; Lim et al., 2019; Mesmin et al., 2013). Ultrastructural examination of mouse and human islet β-cells using transmission electron microscopy revealed the presence of ribosome-free ER domains in close proximity to insulin SGs (Fig. 3A,B). To obtain a more detailed view of these contacts we performed volumetric reconstruction of individual ER-granule contacts in FIB-SEM data of mouse β-cells. We frequently observed ribosome-free ER in close proximity (10-20 nm) to insulin-containing SGs, and in many cases the ER traced the outlines of the granules in a pattern resembling contacts the ER makes with other vesicular organelles (Fig. 3C,D). To further demonstrate the existence of physical contacts between ER and SGs, we performed proximity ligation assays on clonal MIN6 β-cells, mouse and human islets using antibodies against the IP3 receptor (ER) and Rab3 (SGs). This resulted in the appearance of fluorescent puncta in the cytosol of the cells, indicating locations where the ER and SGs are within 20 nm of each other (Fig. 3E-G and Suppl. Fig. 3). Interestingly, we observed more puncta in primary human cells than in clonal cells, perhaps reflecting higher SG density in these cells. Next, we wanted to determine if these contacts existed in live cells and to explore their putative dynamics. We therefore developed a proximity sensor based on dimerization-dependent fluorescent proteins (Alford et al., 2012). This sensor makes use of two quenched monomers, RA and GB, that form a fluorescent heterodimer when brought in proximity to each other. To test the applicability of this method for visualization of membrane contact sites, we designed a version for reporting ER-PM contact sites by targeting RA to the surface of the ER using Sec61β and GB to the plasma membrane through C-terminal lipidation (GB-CaaX). When expressed alone, GB-CaaX showed no detectable fluorescence while RA-Sec61β showed very weak fluorescence that overlapped with that of the ER, consistent with previous work showing incomplete quenching of RA fluorescence (Suppl. Fig. 3) (Alford et al., 2012). Co-expression resulted in distinct fluorescence that was restricted to the cell periphery and overlapped with an ER marker (Suppl. Fig. 4). To determine at what distance from each other the two moieties must be in order to reconstitute a fluorescent protein, we fused GB to the N- or C-terminus of ER-localized E-Syt3 and expressed it together with RA-CaaX. Whereas C-terminally localized GB interacted with RA at the plasma membrane, we could not detect any fluorescence signal from cells expressing N-terminally-localized GB (Suppl. Fig. 4). Based on the structure of E-Syt2 (Schauder et al., 2014), we therefore believe that RA and GB must

be <20 nm from each other, which is a typical inter-membrane distance at MCS (Scorrano et al., 2019). We next localized GB to the surface of SGs by fusing it to Rab3a, and co-expressed it with RA-Sec61β (Fig. 4A). This resulted in strong punctate fluorescence which overlapped with markers of both the ER (ER-oxGFP) (Fig. 4B,C) and SGs (NPY-mNG) (Fig. 4E,F). Whereas all contacts overlapped with the ER marker, only a subset of SGs showed overlap (Fig. 4D,G). The overlap with SGs was highest close to the plasma membrane, where a majority of granules was in contact with the ER, while granules located more centrally in the cell exhibited fewer contacts with the ER (Suppl. Fig. 4). This demonstrates the existence of a granular subpopulation defined by physical tethering to the ER. Time-lapse imaging revealed that the contacts were dynamic and moved together with SGs, indicating physical tethering, and not just proximity, to the ER (Fig. 4H). We next co-expressed the ER-SG proximity reporter with OSBP-Halo$_{JF646}$ and VAPA-mNG. As expected, there was little overlap between OSBP and ER-SG contacts under resting conditions, but OSBP rapidly stabilized at the contact sites upon addition of 20 nM OSW-1 (Fig. 4I). Importantly, treatment with OSW-1 did not change the number of SGs in proximity to the ER, indicating that OSBP becomes stabilized at pre-existing contacts (Fig. 4J,K). To further confirm OSBP and VAP-A localization to ER-SG sites, we again took advantage of the dimerization-dependent fluorescent protein. We made a version where OSBP was fused to the non-fluorescent GB-subunit and co-expressed this together with RA-Sec61β and a SG marker (NPY-mNG) in MIN6 β-cells. Under resting conditions there was essentially no red fluorescence overlapping with the location of SGs. Addition of 20 nM OSW-1 resulted in the rapid appearance of fluorescent puncta that overlapped with, or were in close proximity to, SGs, demonstrating that OSBP becomes enriched at locations where SGs are within 20 nm of the ER (Fig. 4L,M). When co-expressing OSBP-GB and Rab3-RA, we instead observed strong punctate localization already under resting condition, which became more pronounced after OSW-1 addition (Fig. 4N). These structures colocalized with mNG-VAP-A in what appears to be stable complexes, as they exhibit coordinated movements in the cells (Fig. 4N). Together, these observations show that OSBP and VAP-A interact at, but do not induce formation of, ER-SG contact sites.

Coordination of OSBP and Sac2 on the surface of SGs controls insulin secretion

Cholesterol overloading of SGs results in impaired insulin secretion, at least in part due to reduced SG docking at the plasma membrane (Bogan et al., 2012). We recently showed that loss of Sac2 also suppressed insulin secretion by interfering with SG docking (Nguyen et al., 2019), and therefore hypothesized here that the PI(4)P accumulation on SGs seen after Sac2 knockdown may result in excessive accumulation of OSBP at the granule surface with cholesterol overloading as a consequence. siRNA mediated knockdown of OSBP in MIN6 β-cells (Fig. 5A,B) resulted in a slight reduction in intracellular cholesterol accumulation, as determined by filipin staining (Fig. 5C,D). Sac2 knockdown, as described above, instead resulted in increased cholesterol accumulation, which was normalized by simultaneous silencing of OSBP expression (Fig. 5C,D). To test if the Sac2 and OSBP-dependent changes in intracellular cholesterol had an impact on insulin secretion, we determined the effect of Sac2 or OSBP knockdown on depolarization-induced insulin secretion using an optical assay based on VAMP2-pHluorin and TIRF microscopy. Consistent with previous studies, both Sac2 KD and OSBP KD resulted in reduced insulin secretion (34% and 16%, respectively; Fig 5E,F) (Nguyen et al., 2019). Simultaneous Sac2 and OSBP knockdown suppressed secretion to the same extent as OSBP knockdown alone (24%), and secretion was still significantly lower than under control conditions (Fig. 5E,F). Similar results were obtained when glucose-stimulated insulin secretion was assessed using ELISA. siRNA-mediated knockdown of Sac2 reduced the secretory response to 55% of control ($P<0.001$), and

simultaneous knockdown of OSBP did not restore the response to the level of control cells (Fig 5G). Insulin content was unaffected by both Sac2 and Sac2/OSBP knockdown, indicating that the reduction in insulin secretion is due to impaired release and not production (Fig. 5H). To more acutely test the involvement of OSBP in the regulation of insulin secretion we incubated MIN6 cells with OSW-1 (20 nM) for 30 min and assessed the effect on depolarization-induced insulin secretion by ELISA. This timepoint was chosen because it is shorter than the time required for de novo synthesis of insulin SGs at the TGN (Davidson et al., 1988), ruling out potential effects of OSW-1 treatment on SG biogenesis. We found that OSBP inhibition suppressed insulin secretion by 26±9% (Fig. 5I) but was without effect on the voltage-dependent Ca^{2+} influx (Fig. 5J). OSW-1 also inhibited glucose-stimulated insulin secretion from isolated mouse pancreatic islets, but was without effect on glucose-induced Ca^{2+} influx in the same islet preparation (Fig. 5K-M). These results show that lipid transport by OSBP is involved in the acute regulation of insulin secretion downstream of SG formation at the Golgi. The findings are consistent with a cooperative action between Sac2 and OSBP on the surface of SGs of importance for normal insulin secretion.

OSBP localization to SGs is regulated by Ca^{2+} and cytosolic pH

Although constitutive contacts between the ER and SGs are abundant, OSBP is likely not a major component of these, since it primarily localized to the Golgi under resting conditions. The addition of OSW-1 induced accumulation of OSBP at SGs (see Fig. 4L), indicating that there is a constitutive weak or transient interaction between OSBP and SGs that can be stabilized by preventing lipid exchange. We next asked whether OSBP enrichment at SGs might be promoted under certain conditions. The binding of OSBP to the Golgi is counteracted by increases in the cytosolic Ca^{2+} concentration, likely through the inhibition of PI4-kinases at the Golgi with accompanying reduction in Golgi PI(4)P (Balla et al., 2008; Malek et al., 2021). Ca^{2+} is a key second messenger in β-cells, and glucose stimulation causes voltage-dependent Ca^{2+} influx that triggers insulin granule exocytosis. To test if voltage-dependent Ca^{2+} influx had an impact on OSBP distribution, we depolarized MIN6 β-cells expressing OSBP-GFP or OSBP-$Halo_{646}$. We found that Ca^{2+} influx triggered the immediate dissociation of OSBP from the Golgi, and the process was reversed when the depolarizing agent was removed (Fig. 6A,B and Suppl. Fig. 5). TIRF microscopy imaging of MIN6 β-cells expressing OSBP-GFP and the ER-marker Sec61β-mRFP or the granule marker NPY-mCherry showed the appearance of OSBP puncta after depolarization or glucose-stimulation that overlapped with the ER marker and also accumulated around SGs (Suppl. Fig. 5). Similar displacement was also seen in response to Ca^{2+} release from the ER triggered by the addition of carbachol (Suppl. Fig. 6). These experiments show that Ca^{2+} elevations trigger the release of OSBP from the Golgi, perhaps making it available at other membrane contact sites. PI(4)P was recently shown to act as a pH sensor through protonation at acidic pH, which resulted in reduced affinity for effector proteins (Shin et al., 2020). Depolarization of β-cells is associated with acidification of the cytosol (Salgado et al., 1996), and we therefore tested if pH changes may contribute to OSBP displacement from the Golgi. To accomplish rapid pH changes we exposed MIN6 cells loaded with the pH-sensitive dye BCECF to 10 mM NH_4Cl. This caused a rapid alkalinization, seen as an increase in fluorescence. Washout of NH_4Cl resulted in transient acidification that was followed by pH-normalization at the pre-stimulatory level within 1 min (Fig. 6C). Subsequently, we exposed MIN6 cells expressing OSBP-GFP and loaded with the Ca^{2+} indicator Cal590 to 10 mM NH_4Cl. The acute alkalization was without effect on both cytosolic Ca^{2+} and OSBP localization, while washout of NH_4Cl caused dramatic dissociation of OSBP from the Golgi without accompanying change in cytosolic Ca^{2+} (Fig. 6D,E). Importantly, alkalinization of the cytosol with 10 mM NH_4Cl completely prevented the depolarization-induced dissociation of OSBP from the Golgi

while only slightly suppressing the rise of cytosolic Ca^{2+} (Fig. 6D,E). Next, we co-expressed OSBP-GFP and the SG marker NPY-mCherry in MIN6 cells and imaged them with TIRF microscopy. Depolarization resulted in an enrichment of OSBP at SGs which was counteracted by alkalinization of the cytosol with NH_4Cl, indicating that Ca^{2+} increases facilitate the interaction between OSBP and granules, at least in part through acidification of the cytosol (Fig. 6F-J). Importantly, we found that acute addition of the OSBP inhibitor OSW-1 was associated with an acidification of the cytosol, seen as a drop in fluorescence intensity of cytosolically expressed pHluorin, implicating either roles of OSBP in pH regulation or off-target effects of the compound that may contribute to the redistribution of the protein.

DISCUSSION

This work is an extension of our previous study demonstrating an involvement of the PI(4)P phosphatase Sac2 in SG docking and release. We find that the increase in SG PI(4)P that occurs as a consequence of reduced Sac2 expression is paralleled by the accumulation of cholesterol. This accumulation is caused by recruitment of the PI(4)P/cholesterol exchange protein OSBP to the surface of SGs, where it participates in the formation of ER-SG contact sites through interactions with ER-localized VAP proteins and PI(4)P on the granule surface. siRNA-mediated knockdown of Sac2 or OSBP, as well as pharmacological inhibition of OSBP, all resulted in impaired insulin secretion. Together, these results show for the first time the existence of physical contacts between the ER and SGs, and demonstrate that these are sites of lipid transfer of importance for normal insulin secretion.

The cholesterol concentration in the ER is only around 5 mol% of membrane lipids (Van Meer et al., 2008), but it increases in the Golgi, at least in part through the action of OSBP. Mature insulin SGs are estimated to contain ~35 mol% cholesterol (Galli et al., 2023; Tsuchiya et al., 2010), comparable to concentrations found in the plasma membrane (Van Meer et al., 2008). Given that a typical β-cell contains around 10,000 SGs with a total surface area 4.5 times larger than the plasma membrane (Sato Tamiko, 1981), the granule pool of cholesterol represents a major storage site of the lipid in β-cells. The importance of cholesterol for normal insulin secretion has been extensively studied. For example, cholesterol depletion alters glucose metabolism and interferes with the localization of ion channels and SNARE proteins, leading to aberrant insulin secretion regulation (Tsuchiya et al., 2010; Vikman et al., 2009), whereas cholesterol overloading leads to docking and exocytosis defects (Bogan et al., 2012; Hao et al., 2007). Cholesterol transport within β-cells is also important for normal insulin secretion. Both ABCG1 and ABCA1 cholesterol transporters are involved in SG biogenesis, and loss of these transporters leads to cholesterol accumulation and impaired insulin secretion, at least in part by destabilizing the SGs, resulting in their lysosomal degradation (Hussain et al., 2018; Kruit et al., 2010). The ABC cholesterol transporters do not localize to SGs and it is generally assumed that cholesterol loading occurs prior to granule departure from the trans-Golgi network (Harris et al., 2018). OSBP, another cholesterol transport protein found at membrane contact sites, has also been shown to positively regulate insulin secretion, but its cellular localization in β-cell is not known (Hussain et al., 2018). We now confirm that loss of OSBP activity results in reduced insulin secretion. We also find that OSBP associates with a fraction of SGs, likely via an interaction between its PH-domain and PI(4)P on the granule surface (Levine and Munro, 2002). The phosphatase Sac2 negatively regulates PI(4)P levels on SGs (Nguyen et al., 2019), and knockdown of Sac2 resulted in accumulation of granule PI(4)P and in excess cholesterol loading that could be normalized by simultaneous OSBP knockdown. Acute inhibition of

OSBP with OSW-1 (Burgett et al., 2011) resulted in redistribution of both OSBP and its ER-localized receptor VAP-A to SGs. OSBP is not strongly attached to target membranes, and efficient lipid transport depends on dynamic equilibrium between membrane-bound and free molecules and arises, as least in part, as a consequence of OSBP extracting the same lipid (PI[4]P) that it uses for membrane tethering (Mesmin et al., 2013; Mesmin et al., 2017). When the exchange of lipids is prevented by OSW-1, this results in stabilization of OSBP at PI(4)P-rich membrane structures, in this case insulin SGs. In addition to PI(4)P-binding, OSBP-mediated contacts typically depend on a co-receptor. At the endosomes, VAP-A is recruited through an interaction with SNX9 and PI(3)P, in addition to OSBP and PI(4)P (Dong et al., 2016). Interaction with the Golgi instead depends on Arf1-GTP and PI(4)P (Levine and Munro, 2002). Association with SGs likely also requires a coreceptor, since we can stabilize OSBP at SGs by the low affinity association between the two dimerization-dependent RFP moieties (see Fig. 4J). Such a coreceptor mechanism is in place in yeast cells, where the OSBP homologue Osh4p binds to secretory granules in a manner that depends on the 4'-phosphatase Sac1 (Ling et al., 2014). The regulation of OSBP localization by Sac2 may be a way to avoid cholesterol overloading of SGs, where the enzyme-mediated removal of PI(4)P act as a break on cholesterol transport (see Fig. 6K). Given that both cholesterol excess and deficiency cause defects in insulin secretion (Bogan et al., 2012; Hao et al., 2007; Vikman et al., 2009; Xia et al., 2008), such negative feedback may be of importance to ensure that SGs accumulate appropriate amounts of cholesterol. However, Sac2 likely regulates insulin secretion also distal to cholesterol loading, since simultaneous Sac2 and OSBP knockdown normalized SG cholesterol content but not insulin secretion. A possibility is that other lipid transport proteins operate at ER-SG contact sites in a PI(4)P dependent manner. In fact, most ORPs has PI(4)P as the preferred binding target (Nakatsu and Kawasaki, 2021). One candidate is ORP3, which similar to OSBP is equipped with a PI(4)P-binding PH-domain and a VAP-A-binding FFAT-motif. This protein has been shown to counter-transport PI(4)P and phosphatidylcholine (PC) at ER-PM contact sites (D'souza et al., 2020). SGs contain PC (MacDonald et al., 2015), but it is not known how the levels of this lipid are regulated at this cellular location or what the downstream effectors are. An attractive candidate is PLD1, which catalyzes the formation of phosphatidic acid from PC, localizes to SGs and is required for insulin secretion (Hughes et al., 2004; Ma et al., 2010). It is also possible that the changes in ER-SG contacts brought about by PI(4)P accumulation result in aberrant recruitment of other proteins to these sites. It would for example be of relevance to determine if contacts between ER-localized STIM1 and granule-localized Orai1 can form in response to changes in ER Ca^{2+} and contribute to cellular Ca^{2+} homeostasis, similar to what has been shown in other secretory cells (Dickson et al., 2012). Insulin-containing SGs represent a significant Ca^{2+} store in β-cells that also contribute to insulin secretion, although through what mechanisms remains unknown (Idevall-Hagren and Tengholm, 2020; Mitchell et al., 2001).

OSBP is primarily engaged in lipid transport at the ER-Golgi interface under resting conditions, yet OSBP has been show to participate in similar reactions at other membrane contact sites under different physiological and pathophysiological conditions (Nakatsu and Kawasaki, 2021). Mechanisms that control OSBP redistribution and dynamics are still poorly understood, but it has been shown that Ca^{2+} can displace OSBP from the Golgi (Balla et al., 2008; Malek et al., 2021). We now show that elevation of the cytosolic Ca^{2+} concentration, together with the ensuing acidification, resulted in weak displacement of OSBP from the Golgi but also in enhanced association between OSBP and SGs, at least in the sub-plasma membrane space of the β-cell. This is reminiscent of OSBP inhibition with OSW-1, which stabilizes the interaction between OSBP and SGs. How Ca^{2+} stabilizes OSBP at SGs and

whether it is coupled to displacement of OSBP from the Golgi is not clear. Displacement of OSBP from the Golgi also occurred following inhibition of PI4-kinases, but this did not result in accumulation of OSBP at SGs, indicating either that PI4-kinase are required to maintain granule PI(4)P levels or that Ca^{2+}/pH promote the association trough additional mechanism. Such mechanism may involve pH-mediated changes in PI(4)P protonation (Shin et al., 2020), direct effects of Ca^{2+} on OSBP (Malek et al., 2021) or PI(4)P (Kang et al., 2017) as well as pH or Ca^{2+} induced clustering of PI(4)P in the target membrane which may increase the apparent affinity for the PH-domain of OSBP (Redfern and Gericke, 2004; Sarmento et al., 2014). Irrespective of mechanism, the spatial control of OSBP by Ca^{2+} couples lipid exchange at the SG surface to Ca^{2+}-triggered exocytosis of SGs. Consistently, we find that acute inhibition of OSBP activity suppresses insulin secretion, indicating that OSBP acts immediate upstream of the exocytic process and distal to the formation of SGs at the Golgi. Further support for this notion comes from our observation that both ER contacts and OSBP binding preferentially involves SGs located close to the plasma membrane. These physically docked granules are preferentially released in response to depolarization or during the first phase of glucose-stimulated insulin secretion, and both these mechanisms are also suppressed by OSBP inhibition. In addition to being physically docked at the plasma membrane, these SGs also represent a subpopulation of granules that has recently been formed at the trans-Golgi network (Ivanova et al., 2013). It is therefore tempting to speculate that cholesterol transport at ER-SG contacts represents an important step in the maturation of newly formed SGs. Consistent with this notion, it has been shown that newly formed post Golgi secretory vesicles are enriched for ergosterol and has a higher membrane order than the late Golgi membranes (Klemm et al., 2009).

To conclude, we propose a model where glucose-induced increases in Ca^{2+}, together with the ensuing acidification, facilitate interactions between OSBP and SGs. OSBP then participates in the controlled loading of cholesterol to the SG membrane in cooperation with the granule-localized PI(4)P phosphatase Sac2 in a process that is required for normal insulin secretion. OSBP interacts with granules at ER-SG contact sites, but does not seem to be involved in the formation of these contacts. Future research should aim at identifying protein complexes and biological processes that occurs at these largely uncharacterized membrane contact sites.

ACKNOWLEDGEMENTS

We are grateful for the expert technical assistance provided by Dr. Beichen Xie, Ms. Cornelia Carleson and Mrs. Antje Thonig. OI was supported by grants from The Swedish Research Council (MH-2019-01456); The Novo-Nordisk Foundation (NNF19OC0055275), Åke Wibergs stiftelse (M18-0146), Diabetesfonden (DIA2018-332), Magnus Bergwalls stiftelse (2018-02752), Familjen Ernfors stiftelse, EFSD/Lilly and EXODIAB. MS was supported with funds from the German Center for Diabetes Research (DZD e.V.) by the German Ministry for Education and Research (BMBF) and from the Innovative Medicines Initiative 2 Joint Undertaking under grant agreement No 115881 (RHAPSODY) and the Swiss State Secretariat for Education, Research and Innovation (SERI; 16.0097-2). AM was the recipient of a MeDDrive grant from the Carl Gustav Carus Faculty of Medicine at TU Dresden. LE received support from The Swedish Research Council (2019-01406). AT received support from The Swedish Research Council (2021-02081), Swedish Diabetes Foundation, Diabetes Wellness Foundation, Family Ernfors Foundation, Nils Erik Holmsten's Foundation, Novo-

Nordisk Foundation and the Swedish national strategic grant initiative EXODIAB (Excellence of diabetes research in Sweden).

FIGURES AND LEGENDS

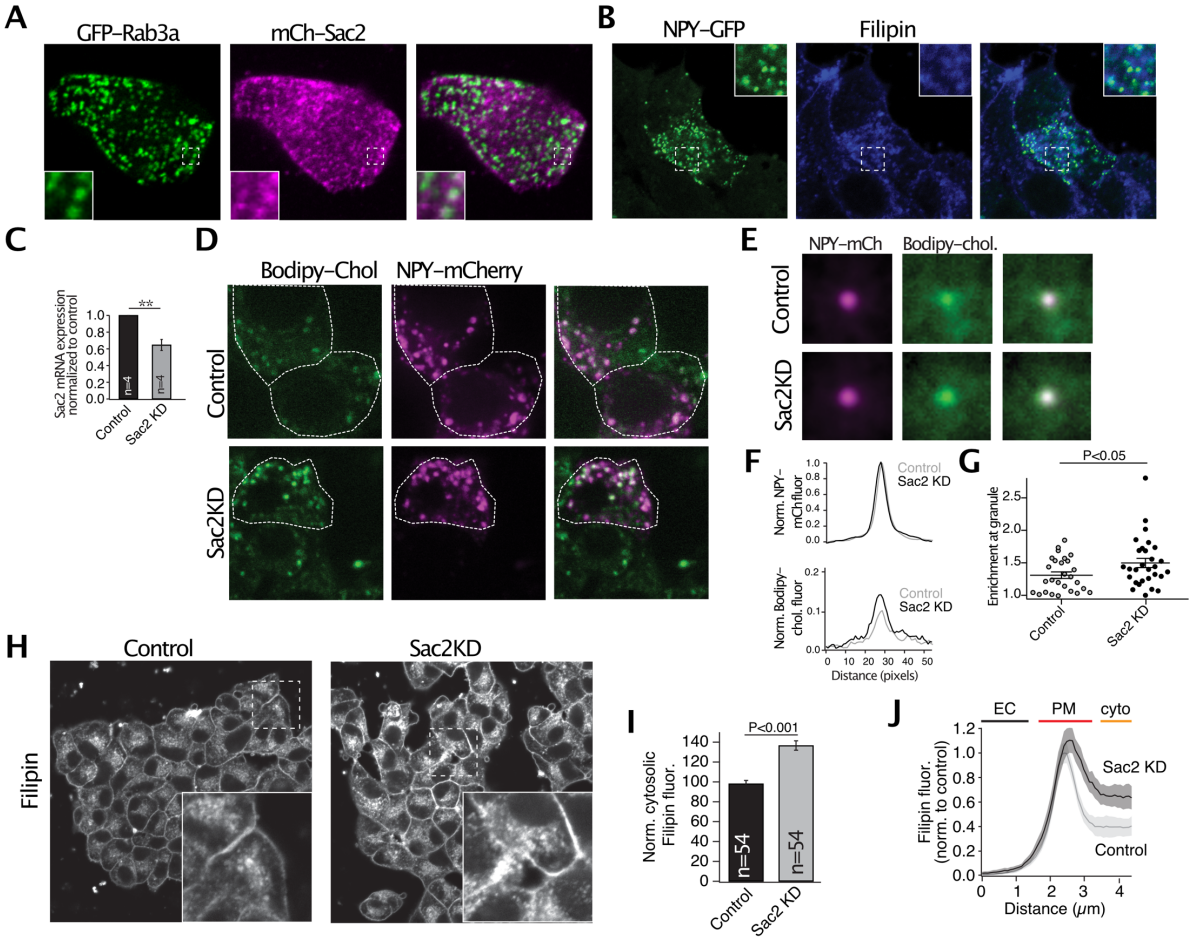

Figure 1. Sac2 knockdown results in cholesterol accumulation on insulin granules. **A.** Confocal microscopy images of a MIN6 cells expressing the granule marker GFP-Rab3a (green) and mCherry-Sac2 (magenta). **B.** immunofluorescence image of MIN6 cells expressing NPY-GFP (green) and stained with filipin (blue) to visualize cholesterol. **C.** Quantitative RT-PCR determination of Sac2 mRNA levels in control and Sac2 knockdown cells expressed relative to control after normalization to GAPDH mRNA levels (n=4, ** P<0.01). **D.** Confocal microscopy images of NPY-mCherry-expressing MIN6 cells loaded with fluorescent cholesterol (Bodipy-cholesterol). Top panel shows cells transfected with control siRNA and bottom panel shows cells transfected with siRNA against Sac2. **E.** Confocal microscopy images showing the average accumulation of Bodipy-cholesterol fluorescence at NPY-mCherry positive structures in control cells or Sac2 knockdown cells. Images are averages of 270 and 290 structures from 27 and 29 cells. **F.** Traces showing intensity profiles from the averaged images in E plotted using a diagonal line with the granule in the center. Top shows intensity profiles for the granule marker and bottom intensity profiles for the corresponding Bodipy-cholesterol. **G.** Scatter plot showing the enrichment of bodipy-cholesterol at NPY-mCherry positive structures (n=27 cells for control and 29 cells for Sac2 KD). **H.** Confocal microscopy images of control and Sac2 knockdown MIN6 cells stained with the fluorescent cholesterol dye Filipin. Boxed areas are shown as magnifications. **I.** Cytosolic filipin intensity in Sac2 knockdown cells normalized to that of control cells (n=54 cells, ***P<0.001). **J.** Line profiles (mean±S.E.M.) drawn across the plasma membrane in confocal micrographs from filipin-stained control and Sac2 knockdown cells (n=17 cells).

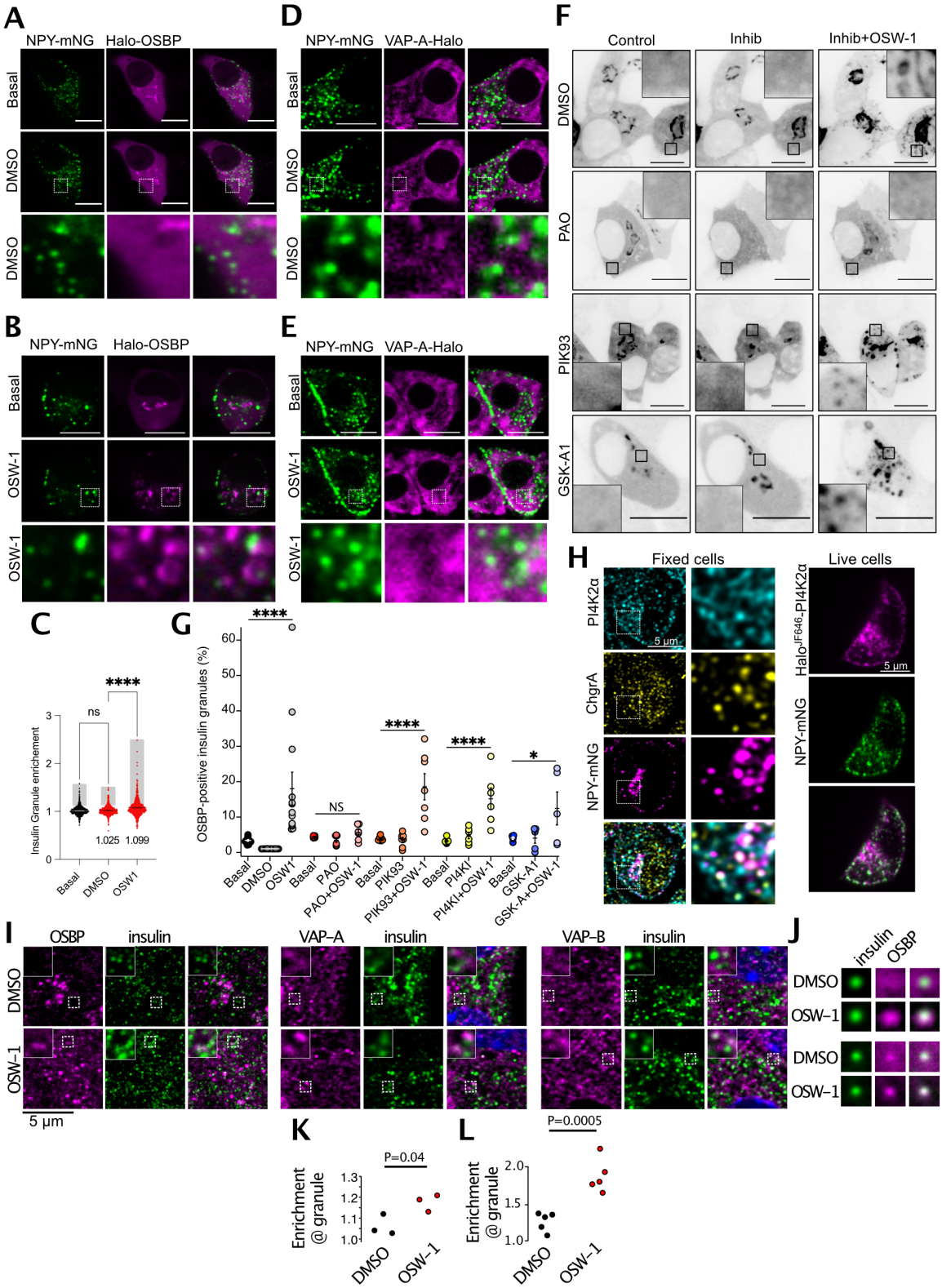

Figure 2. Inhibition of OSBP results in accumulation of OSBP and VAP-A on insulin granules.

A,B. Confocal microscopy images of a DMSO-treated (0.1%; A) or OSW-1-treated (20 nM; B) MIN6 cell expressing the granule marker NPY-mNG (green) and Halo^{JF646}-OSBP (magenta). Bottom rows show magnified areas. **C.** Scatter plot showing the enrichment of OSBP at NPY-mNG positive structures under basal conditions and following incubation with

DMSO (0.1%) or OSW-1 (20 nM). Notice the appearance of a population of granules (shaded area) positive for OSBP following OSW-1 treatment (1123-1289 structures from 6 independent experiments, **** P<0.0001, 2-way ANOVA followed by Tukey's post hoc test). **D, E.** Confocal microscopy images of a DMSO-treated (0.1%; D) or OSW-1-treated (20 nM; E) MIN6 cell expressing the granule marker NPY-mNG (green) and VAP-A-Halo^{JF646} (magenta). Bottom rows show magnified areas. **F, G.** Confocal microscopy images (F) and quantifications (G) showing the accumulation of OSBP on insulin granules following the addition of OSW-1 (20 nM) in the absence or presence of the indicated PI4-kinase inhibitors (N=5-10 independent experiments; **** P<0.0001; 2-way ANOVA with Kuskall-Wallis post hoc test). Scale bar is 5 µm. **H.** Confocal microscopy images of a MIN6 cell immunostained for PI4KIIα (cyan), ChrgA (yellow) and expressing NPY-mNG (magenta). The boxed region is shown as a magnification to the right. To the left are confocal microscopy images of a live MIN6 cell expressing Halo^{JF646}-PI4KIIα (magenta) and NPY-mNG (green). **I.** Confocal microscopy images of mouse islets immunostained for insulin (green) and OSBP, VAP-A or VAP-B (magenta) under control conditions (DMSO; top) or following 30 min incubation with 20 nM OSW-1 (bottom). **J.** Confocal microscopy images showing the average accumulation of OSBP on insulin granules in the presence of DMSO (0.1%) or OSW-1 (20 nM) in MIN6 cells (top) and mouse islet β-cells (bottom). Images are averages of 100 structures from 10 cells. **K, L.** Quantification of the relative enrichment of OSBP on insulin granules in the absence or presence of OSW-1 in MIN6 cells (n=3 experiments; I) and mouse islet β-cells (n=5 experiments; J) (Mann-Whitney U-test). Scale bars are 10 µm.

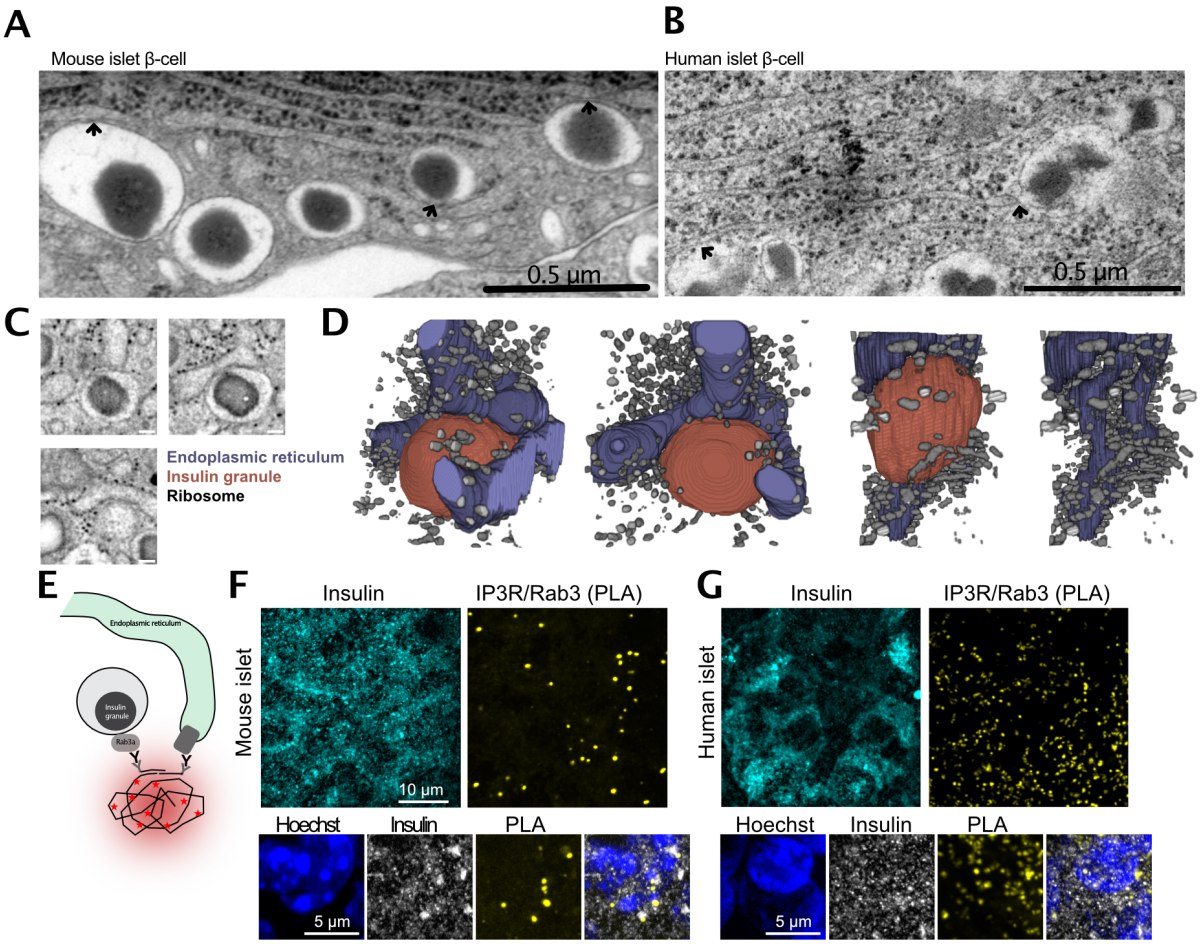

Figure 3. Characterization of ER-insulin granule contact sites
A,B. Transmission electron microscopy image of a mouse (left) and human (right) β-cell showing close proximities between insulin granules and the endoplasmic reticulum (arrows). **C.** x-y slices at different z-positions from FIB-SEM images showing the proximity between an insulin granule and the ER in a mouse β-cell. Scale bar: 100 nm. **D.** Volumetric rendering of the granules in C showing the granule in red, the ER in purple and ribosomes in grey. **E.** Principle of PLA for detection of ER-insulin granule contacts using antibodies against the ER (IP3-receptor) and insulin granules (Rab3a). **F.** Immunofluorescence images of a mouse islet stained for insulin (cyan) and with ER-granule contacts detected with PLA (yellow). Magnified images are shown below. **G.** Immunofluorescence images of a human islet stained for insulin (cyan) and with ER-granule contacts detected with PLA (yellow). Magnified images are shown below.

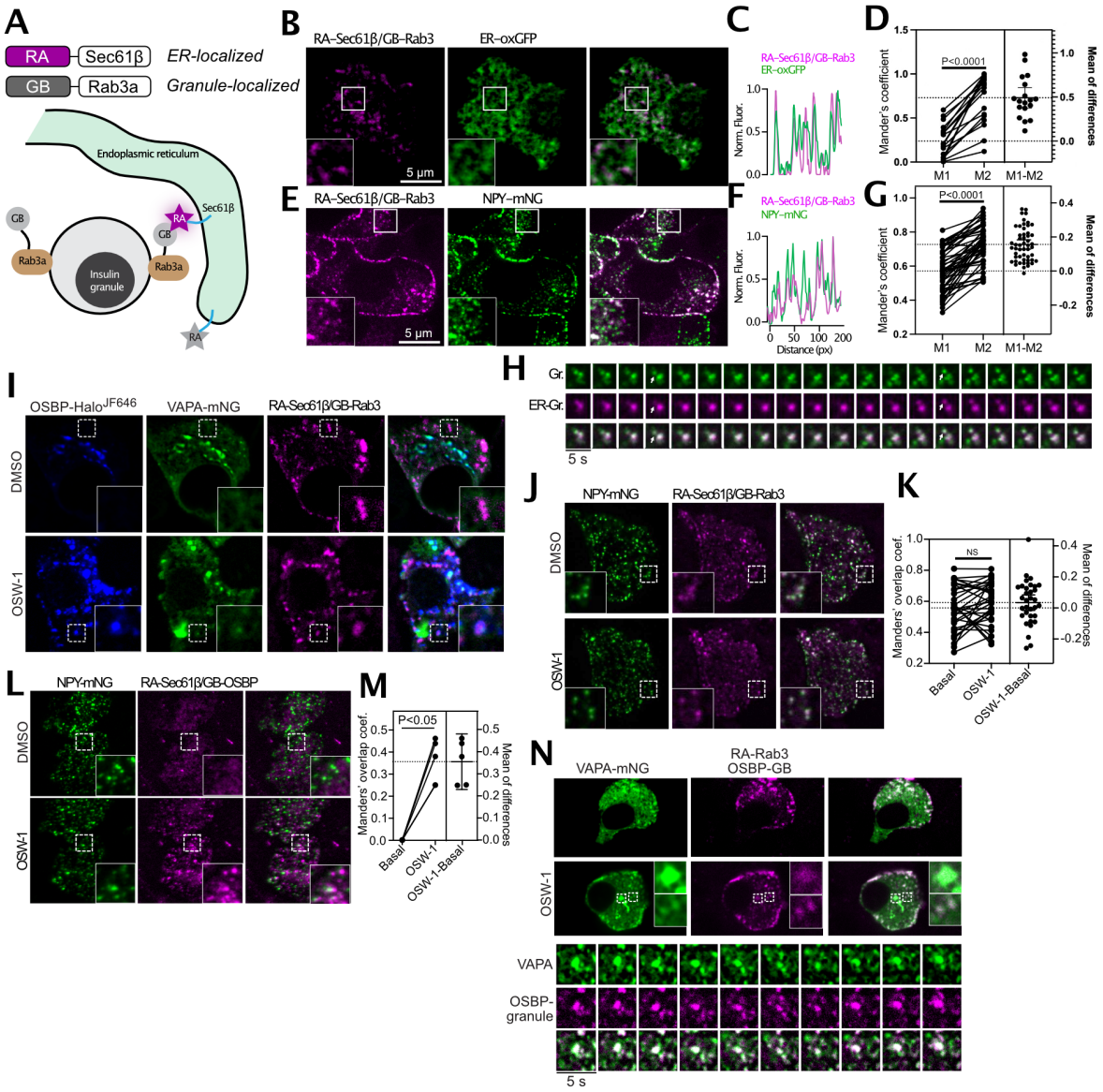

Figure 4. Dynamics of ER-insulin granule contact sites

A. Principle for detection of ER-granule proximity using dimerization-dependent RFP. **B.** Confocal microscopy images of MIN6 cells expressing the ER-granule proximity reporter (RA-Sec61β/GB-Rab3a; magenta) together with an ER-marker (ER-oxGFP). **C.** Line profiles drawn across the cell in B. **D.** Quantification of the colocalization between ER and the contact site reporter (M1) and the contact site reporter and ER (M2) (n=17 cells; 2-tailed Student's t-test). **E.** Confocal microscopy images of MIN6 cells expressing the ER-granule proximity reporter (RA-Sec61β/GB-Rab3a; magenta) together with a granule marker (NPY-mNG). **F.** Line profiles drawn across the cell in B. **G.** Quantification of the colocalization between granules and the contact site reporter (M1) and the contact site reporter and granules (M2) (n=53 cells; 2-tailed Student's t-test). **H.** Images from a confocal microscopy time-lapse recording showing the dynamics of ER-granule contacts (magenta) and insulin granules (green). **I.** Confocal microscopy images of MIN6 cells expressing Halo^{JF646}-OSBP (blue), VAP-A-mNG (green) and the ER-granule contact site reporter in the absence (top) or presence (bottom) of 20 nM OSW-1. **J.** Confocal microscopy images of RA-Sec61/GB-Rab3 (magenta) and NPY-mNG in the absence (top) or presence (bottom) of 20 nM OSW-1. **K.** Quantification of the colocalization between granules and RA-Sec61/GB-Rab3 in the absence (basal) and presence (OSW-1) of 20 nM OSW-1 (n=36 cells; 2-tailed Student's t-test). **L.**

Confocal microscopy images of RA-Sec61/GB-OSBP (magenta) and NPY-mNG in the absence (top) or presence (bottom) of 20 nM OSW-1. **M.** Quantification of the colocalization between granules and RA-Sec61/GB-Rab3 in the absence (basal) and presence (OSW-1) of 20 nM OSW-1 (n=5 cells, Mann-Whitney U-test). **N.** Confocal microscopy images of MIN6 cells expressing VAP-A-mNG (green) and RA-Rab3/OSBP-GB (magenta) in the absence (top) or presence (bottom) of 20 nM OSW-1. Images below show dynamic movements of granule-associated OSBP (magenta) with VAP-A in a cell exposed to OSW-1.

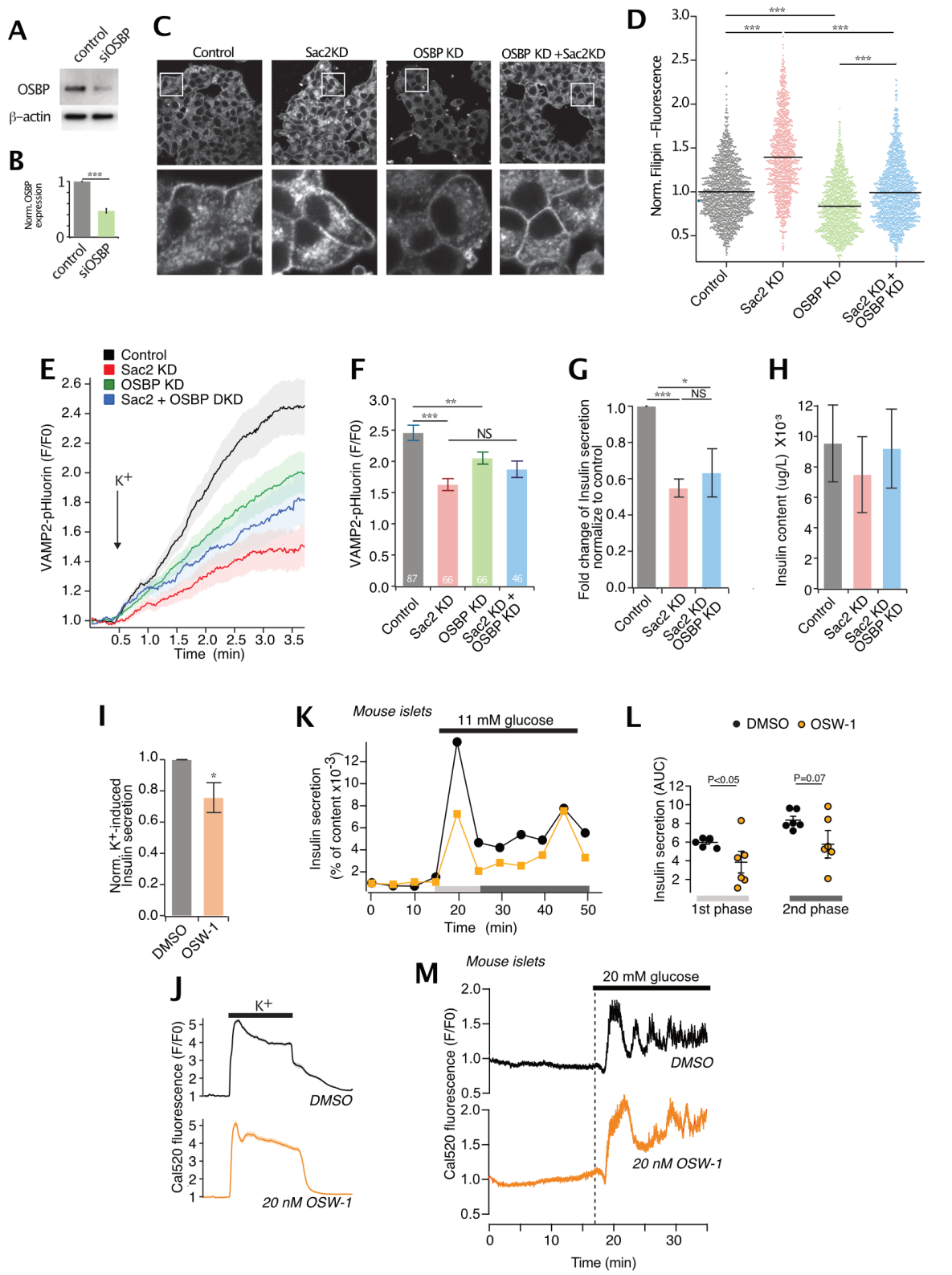

Figure 5. OSBP knockdown or inhibition suppresses insulin secretion

A. Example immunoblot of lysates from MIN6 cells treated with control or OSBP siRNA probes with antibodies against OSBP and β-actin. **B.** Quantifications of OSBP protein levels in MIN6 cells treated with control or OSBP siRNA (expressed relative to β-actin; n=3; *** P<0.001, Mann-Whitney U-test). **C.** Confocal microscopy images of filipin-stained MIN6 cells treated with control siRNA, siRNA against Sac2, OSBP or Sac2+OSBP. **D.** Normalized cytoplasmic Filipin intensity in control MIN6 cells (n=1604) or MIN6 cells treated with

siRNA against Sac2 (n=1176), OSBP (n=1266) or Sac2+OSBP (n=1492) (*** P<0.0001; ANOVA followed by Tukeys post hoc test). **E.** TIRF microscopy recordings of VAMP2-pHluorin fluorescence change in response to 30 mM K^+ in control cells and cells treated with siRNA against Sac2, OSBP or Sac2+OSBP. Data presented as means±S.E.M. for 47 (control), 31 (sac2 KD), 42 (OSBP KD) and 21 (Sac2+OSBP KD) cells from one experiment. **F.** Means±S.E.M. for the maximum VAMP2-pHluorin fluorescence increase in response to 30 mM K^+ in the indicated cells. Data from 87 (control), 66 (Sac2 KD), 66 (OSBP KD) and 46 (Sac2+OSBP KD) cells from three experiments (** P<0.01; *** P<0.001, ANOVA followed by Kruskall-Wallis post hoc test). **G.** ELISA measurements of glucose-stimulated insulin secretion from MIN6 cells treated with control siRNA or siRNA against Sac2 or Sac2+OSBP. Data is expressed as fold change in insulin secretion when the glucose concentration was increased from 3 mM to 20 mM and is expressed relative to control cells (averages±S.E.M.; n=5; * P<0.05; *** P<0.001; Mann-Whitney U-test). **H.** Insulin content in control cells or cells treated with control siRNA or siRNA against Sac2 or Sac2+OSBP (averages±S.E.M.; n=5). **I.** ELISA measurement of K^+-induced insulin secretion in DMSO- (control) and OSW-1- (20 nM, 60 min) treated MIN6 cells (n=4; * P<0.05; Mann-Whitney U-test). **J.** Cal520 fluorescence change in response to 30 mM K^+ in DMSO- or OSW-1- (20 nM, 60 min) treated cells (means±S.E.M.; n=100 cells for both conditions; 2-tailed unpaired Student's t-test). **K.** Insulin secretion from mouse islets perfused with the indicated glucose buffers. The islets were pretreated for 30 min with DMSO (0.1 vol%; black) or OSW-1 (20 nM, orange). **L.** Quantification of the first and second phase insulin secretion from the perfused mouse islets in K (n=5 for each condition; Mann-Whitney U-test). **M.** Cal520 fluorescence change in response to 11 mM glucose in DMSO- or OSW-1- (20 nM, 30 min) treated mouse islet β-cells (n=5 islets per condition).

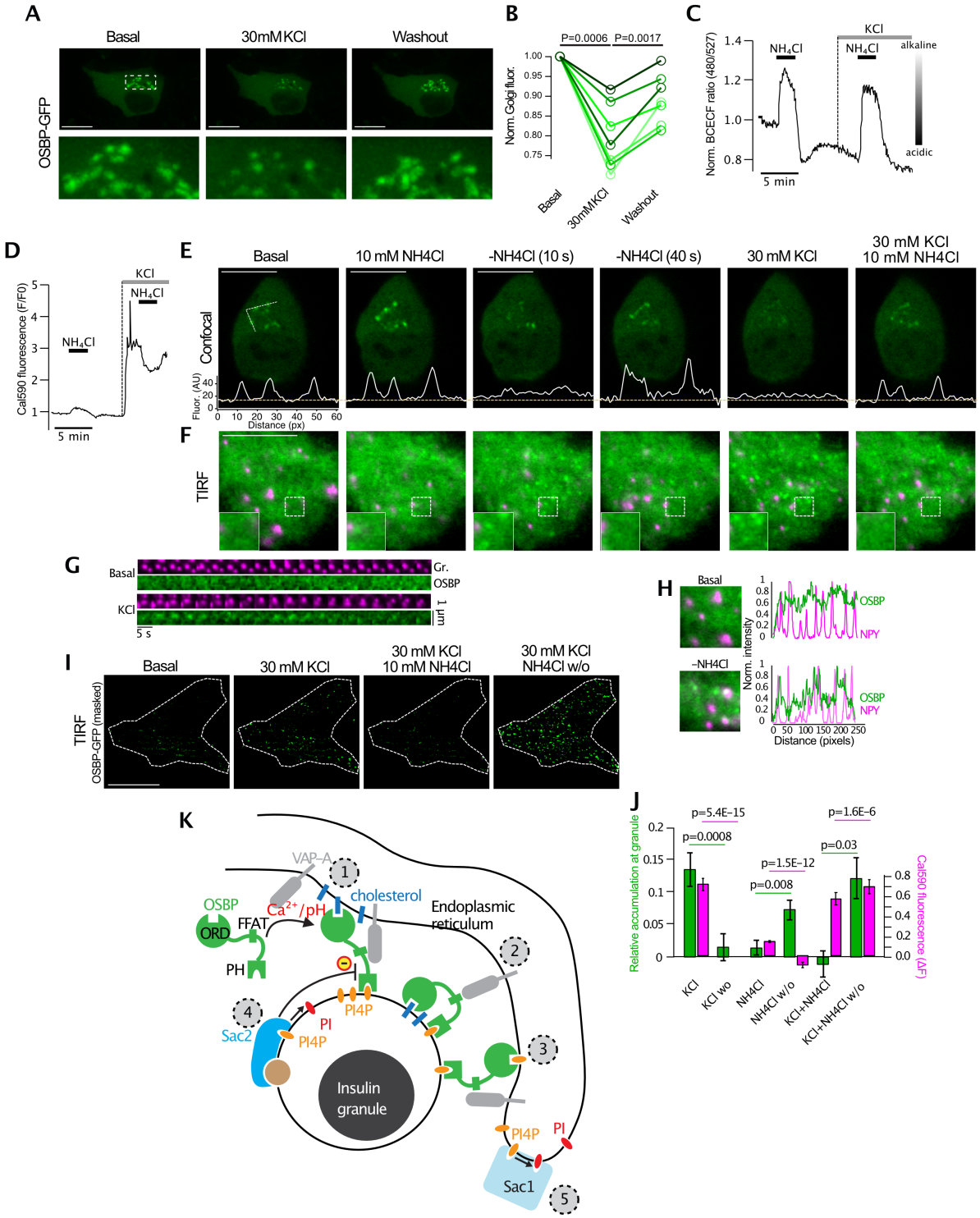

Figure 6. Spatial control of OSBP by Ca^{2+} and cytosolic pH.
A. Confocal microscopy images of a MIN6 cell expressing GFP-OSBP exposed to 30 mM KCl. Images below are magnifications from the boxed are. **B.** Normalized Golgi OSBP-GFP fluorescence before, during and after stimulation with 30 mM KCl (n=7 cells; 2-tailed paired Student's t-test). **C.** Measurements of cytosolic pH in a MIN6 cells loaded with BCECF (representative of 84 cells from 3 experiments). Notice that the addition of KCl causes a slight acidification of the cytosol. **D.** Measurements of cytosolic Ca^{2+} in a MIN6 cell exposed to NH_4Cl (10 mM) or a combination of NH_4Cl and 30 mM KCl (representative of 111 cells from 3 experiments). **E.** Confocal micrographs of a MIN6 cell expressing GFP-OSBP and exposed to the indicated solutions. White line is an intensity profile plot across the Golgi. **F.** TIRF

microscopy images of a MIN6 cells expressing GFP-OSBP (green) and NPY-mCherry (magenta) during stimulation with the indicated solutions. Notice the appearance of small, punctate structures following depolarization and acidification. **G.** Cut-outs showing the dynamic localization of GFP-OSBP to NPY-mCherry-positive granules following depolarization with 30 mM KCl. **H.** TIRF microscopy images (left) and line profiles (right) of cells under basal condition and following washout of NH4Cl. Notice the accumulation of OSBP (green) around insulin granules (magenta). **I.** TIRF microscopy images of a MIN6 cells expressing GFP-OSBP and exposed to the indicated buffers. Images have been masked to highlight the appearance of small punctate structures. **J.** Quantification of the normalized change in cytosolic Ca^{2+} (magenta) and the corresponding enrichment of GFP-OSBP at NPY-mCherry positive granules (green). Notice that acidification causes enrichment of OSBP at granules without corresponding change in Ca^{2+} and that alkalinization of the cytosol with NH_4Cl inhibits KCl-induced enrichment of OSBP on granules (n=10 cells from 3 experiments for OSBP enrichment and n=95 cells from 3 experiments for Ca^{2+} recordings). **K.** Cartoon illustrating the cooperation between granule-localized Sac2 and OSBP in controlling turnover of granular PI(4)P and counter-transport of cholesterol. **1)** OSBP binds to the ER via interactions between the FFAT-motif and VAP-A and to the insulin granule via interactions between the PH-domain and PI(4)P. OSBP extracts a cholesterol lipid from the ER membrane that is harbored within the ORD domain. **2)** The cholesterol lipid is delivered to the insulin granule membrane. **3)** A PI(4)P lipid is extracted from the granule membrane and delivered to the ER membrane. **4)** The association of OSBP with the insulin granule is negatively regulated by the PI(4)P phosphatase Sac2. **5)** PI(4)P delivered to the ER membrane is rapidly dephosphorylated by the PI(4)P phosphatase Sac1. Scalebars are 10 µm.